Microwave Photon-Assisted Incoherent Cooper-Pair Tunneling in a Josephson STM

A. Roychowdhury,[1,2,*] M. Dreyer,[3] J. R. Anderson,[2] C. J. Lobb,[2] and F. C. Wellstood[2]
[1]*Laboratory for Physical Sciences, College Park, Maryland 20740, USA*
[2]*Department of Physics, Center for Nanophysics and Advanced Materials and Joint Quantum Institute, University of Maryland, College Park, Maryland 20742, USA*
[3]*Laboratory for Physical Sciences, College Park, Maryland 20740, USA and Department of Physics, University of Maryland, College Park, Maryland 20742, USA*

(Received 23 March 2015; revised manuscript received 10 July 2015; published 29 September 2015)

We observe photon-assisted Cooper-pair tunneling in an atomic-scale Josephson junction formed between a superconducting Nb tip and a superconducting Nb sample in a scanning tunneling microscope (STM) at 30 mK. High-resolution tunneling spectroscopy data show a zero-bias conduction peak and other sharp subgap peaks from coupling of the STM junction to resonances in the electromagnetic environment. The subgap peaks respond to incident microwave radiation by splitting into multiple peaks with the position and height depending on the frequency and amplitude of the microwaves. The interpeak spacing shows that the charge carriers are Cooper pairs rather than quasiparticles, and the power dependence reveals that the current originates from photon-assisted phase-incoherent tunneling of pairs rather than the more conventional phase-coherent tunneling of pairs that yields Shapiro steps.

DOI: 10.1103/PhysRevApplied.4.034011

I. INTRODUCTION

The use of superconducting (SC) tips instead of normal-metal tips in scanning tunneling microscopy (STM) allows for enhanced spectroscopic resolution due to the singularity in the density of states at the SC gap edge [1–3]. In addition, the ability of a SC tip to probe the pair condensate in a SC sample on the atomic scale has inspired recent interest in Josephson STMs [4–7]. However, pioneering work at 2.1 K with SC tips and samples [8] reveals a resistive zero-bias conductance peak (ZBCP) rather than a true phase-coherent Josephson supercurrent [9] due to classical phase diffusion that is governed by the physics of ultrasmall Josephson junctions (small capacitance and small critical current) [10,11].

In this paper, we present phase-incoherent Cooper-pair tunneling data obtained at millikelvin temperatures in a superconducting Nb-Nb STM junction. Although the tunneling is phase incoherent, we show that the charge of the carriers of $2e$ can be unambiguously determined by applying microwaves to produce photon-assisted tunneling. Since the tunneling current arises from an atomic-scale region, in principle, the technique allows the discrimination of normal regions in highly inhomogeneous SC samples [12–14], the unambiguous detection of small SC regions in otherwise normal-metal samples, and the independent determination of the supercurrent fraction of a localized zero-bias conductance peak or other features that occur in tunneling spectroscopy.

*Present address: Intel Corp., Ronler Acres, 2501 NW 229th Ave, Hillsboro 97124, Oregon.

II. THEORETICAL CONSIDERATIONS

Photon-assisted *quasiparticle* tunneling has been studied extensively in thin-film superconductor-insulator-superconductor (S-I-S) tunnel junctions and single-electron transistors [15–21]. In a junction driven by microwaves of frequency ω, the time-averaged (dc) quasiparticle current through the junction is given by [22]

$$\overline{I_{\mathrm{QP}}(V_0, V_\mu)} = \sum_{l=-\infty}^{\infty} J_l^2\left(\frac{eV_\mu}{\hbar\omega}\right) I_{\mathrm{QP}}\left(V_0 - \frac{l\hbar\omega}{e}\right), \quad (1)$$

where V_μ is the amplitude of the applied microwaves seen by the junction, V_0 is the dc bias voltage across the junction, J_l is the lth Bessel function, and $I_{\mathrm{QP}}(V)$ is the quasiparticle current when no microwave voltage is applied. In contrast, the phase-incoherent, time-averaged Cooper-pair current through an ultrasmall junction that is driven by microwaves at frequency ω is given by [22]

$$\overline{I_s(V_0, V_\mu)} = \sum_{l=-\infty}^{\infty} J_l^2\left(\frac{2eV_\mu}{\hbar\omega}\right) I_s\left(V_0 - \frac{l\hbar\omega}{2e}\right), \quad (2)$$

where $I_s(V)$ is the phase-incoherent Cooper-pair current in the absence of microwaves, and V_μ, V_0, and J_l have the same meaning as in the quasiparticle case.

Phase-incoherent pair tunneling requires an ultrasmall SC junction subject to fluctuations that destroy phase coherence [23]. This limit is easily obtained in a STM junction because of the typically small junction capacitance $C < 1$ fF and critical current $I_c < 1$ nA. In contrast, the

much larger critical current (μA) and capacitance (pF) of typical macroscopic Josephson junctions produces phase-coherent tunneling and inhibits phase-incoherent tunneling of Cooper pairs.

Microwaves incident on a phase-coherent junction produce Shapiro steps due to synchronization of phase oscillations with the incident microwaves [24]. For a voltage-biased macroscopic junction with critical current I_c the time-dependent supercurrent is given by [23]

$$I_s(V_0,t) = \sum_{l=-\infty}^{\infty} (-1)^l J_l\left(\frac{2eV_\mu}{\hbar\omega}\right) I_c \times \sin\left[\gamma_0 + \left(\frac{2eV_0}{\hbar} - l\omega\right)t\right]. \quad (3)$$

Note that when $2eV_0 = l\hbar\omega$, the time dependence disappears, leaving dc-supercurrent Shapiro steps with amplitude $2J_l(2eV_\mu/\hbar\omega)I_c$. While Eq. (3) is superficially similar to Eq. (2), the differences are significant [for example, J_l versus J_l^2 and I_c versus $I_s[V_0 - l(\hbar\omega/2e)]$], making it possible to experimentally distinguish phase-coherent and phase-incoherent tunneling.

In practice, we measure the dc conductance $G(V_0,V_\mu) = d\bar{I}/dV_0$ and obtain from Eq. (2), for example,

$$G_s(V_0,V_\mu) = \sum_{l=-\infty}^{\infty} J_l^2\left(\frac{2eV_\mu}{\hbar\omega}\right) G_s\left(V_0 - \frac{l\hbar\omega}{2e}, 0\right). \quad (4a)$$

When Eq. (1) is used as a starting point, we obtain

$$G_{\mathrm{QP}}(V_0,V_\mu) = \sum_{l=-\infty}^{\infty} J_l^2\left(\frac{eV_\mu}{\hbar\omega}\right) G_{\mathrm{QP}}\left(V_0 - \frac{l\hbar\omega}{e}, 0\right). \quad (4b)$$

In Eqs. (4a) and (4b), the sum over l may be interpreted as microwaves causing an energy level ϵ to split into levels $\epsilon \pm l\hbar\omega$ corresponding to the absorption or emission of l photons of frequency ω. The equations also imply that a slowly varying $G(V_0,0)$ versus V_0 curve will exhibit little change in appearance due to microwave radiation. On the other hand, a $G(V_0,0)$ versus V_0 characteristic with features that are sharp compared to $\hbar\omega/ne$ will respond under microwave radiation by developing features shifted by $\hbar\omega/ne$ along the voltage axis, where ne is the charge of the carriers. Thus, for tunneling Cooper pairs, a sharp feature in the $G(V_0,0)$ curve will be shifted in voltage by increments of $\hbar\omega/2e$ when microwaves are applied or by twice this spacing in the quasiparticle case.

It should be pointed out that the range $\pm V_0$ for which the junction responds to microwaves is not a function of carrier charge or frequency but, rather, is approximately equal to the microwave amplitude. It is, therefore, necessary to resolve the fine structure to distinguish the charge. Figure 1(a) shows a simulation of splitting a sharp ZBCP. Here, the 12.5-μV peak width is half of the microwave-induced energy-level spacing for quasiparticles. The difference between pair tunneling (red) and quasiparticle tunneling (blue) is clearly visible. Figure 1(b) shows a borderline case where the width of the ZBCP is comparable to the quasiparticle levels. In Fig. 1(b), a presumed Cooper-pair current will no longer show a clear split-peak structure while the quasiparticle current still does. A slight increase in peak width will wipe out this structure making the cases virtually indistinguishable. A sharp peak and a high-energy resolution compared to the microwave frequency are, thus, necessary to distinguish the carrier charge. In addition, by fitting to the weighted sum of the supercurrent and quasiparticle current, i.e.,

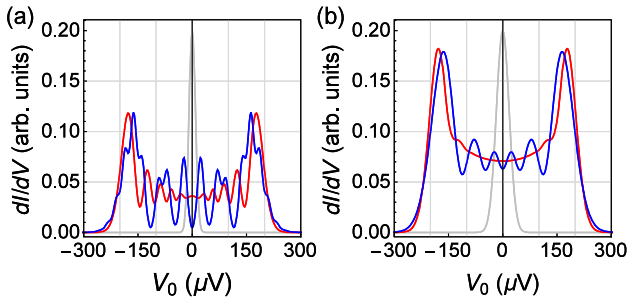

FIG. 1. Simulated splitting of a single Gaussian zero-bias conductance peak (gray) due to microwaves when the charge carriers are Cooper pairs (red) or quasiparticles (blue). The microwave frequency and amplitude are $\omega/2\pi = 5.6$ GHz ($\hbar\omega/e \approx 23$ μeV) and $V_\mu = 200$ μV for both plots. The width of the peak is chosen as 12.5 μV (a) and 25 μV (b), respectively. The height of each ZBCP is scaled by a factor of 1/5 to fit in the same plot.

$$G(V_0,V_\mu) = a_{\mathrm{QP}}G_{\mathrm{QP}}(V_0,V_\mu) + a_sG_s(V_0,V_\mu), \quad (5)$$

it is possible to determine the quasiparticle and supercurrent fractions when both carriers are present. In simulations, we find that fractions as low as 0.01% can easily be discerned. In practice, the noise level of the data determines the detection limit. For all the data shown in this paper, the quasiparticle current fraction is below the detection limit of approximately 2%.

Fortuitously, sharp features are expected in ultrasmall *S-I-S* junctions if the junction is connected to bias leads that have transmission-line resonances or other microwave resonances. When resonances exist, theory predicts the probability $P(E)$ for energy E to be transferred from the tunneling charges to the circuit [25,26], leading to conductance peaks. To achieve the energy resolution necessary to observe these fine-scaled features and the response to microwaves, we cool the STM [27] to 30 mK.

III. EXPERIMENTAL SETUP

Figure 2 shows a photograph of our STM and a simplified schematic of our measurement setup. The

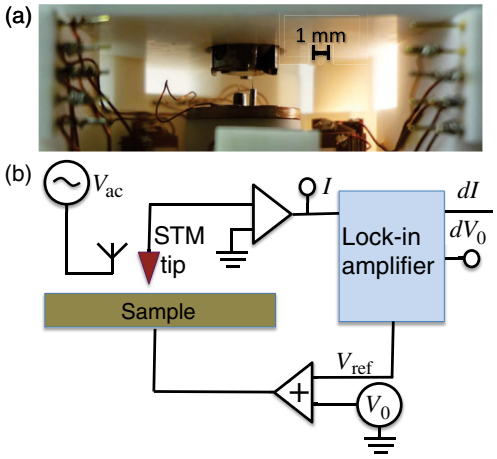

FIG. 2. (a) Photograph of the STM with two Nb tips and a Nb(100) sample. (b) Simplified schematic of experimental setup [28]. V_{ac} is the amplitude of the applied microwaves at the source, I is the tunnel current output, V_0 is the dc bias voltage, and V_{ref} is a 1.973-kHz sinusoidal reference from the lock-in amplifier. The coupling of the microwaves to the STM tip is represented as an antenna.

STM has two independent tips ("inner" and "outer") and is mounted on a custom Oxford Instruments dilution refrigerator [27]. Both tips are cleaned by high-voltage field emission on a gold single crystal at low temperatures before changing to the Nb sample. Microwave power [29] is transmitted indirectly to the STM tips via a dc thermometer line. A lock-in amplifier [30] is used to measure the conductance ($G = d\bar{I}/dV_0$) as a function of the dc bias V_0. The bulk Nb(100) sample is prepared by heating it to 600 °C in ultrahigh vacuum for 10–12 h at a time, while sputtering it with 2-keV Ar^+ ions for nine consecutive days. Once residual polishing grains are removed, the sample is sputtered with 1-keV Ar^+ ions at a temperature of 600 °C for 2–3 h before transferring it to the STM without breaking vacuum [27].

A topographic image of the resulting surface is shown in Fig. 3(a). Since the maximum heating temperature is relatively low, the sample does not show a clear monoatomic step structure as one would expect from a single crystal. However, we find small flat areas [yellow circle in Fig. 3(a)] to conduct spectroscopic measurements. Figures 3(b) and 3(c) show the *S-I-S* gap in $I(V)$ as well as dI/dV spectroscopy. The subgap structure is only visible at smaller tip-sample separation as shown in Figs. 3(d) and 3(e). Figures 3(b) and 3(c) allow measurement of $\Delta_{S\text{-}I\text{-}S} = \Delta_{tip} + \Delta_{sample}$, while Figs. 3(c) and 3(d) give the smaller of the tip and sample superconducting gap. Typically [31], we expect the tip to have the smaller gap. Hence, from $\Delta_{S\text{-}I\text{-}S} = 2.08$ meV and $\Delta_{tip} = 0.61$ meV, we find $\Delta_{sample} = 1.47$ meV. Similar characterizations are performed prior to each microwave-power-dependent series presented in this paper.

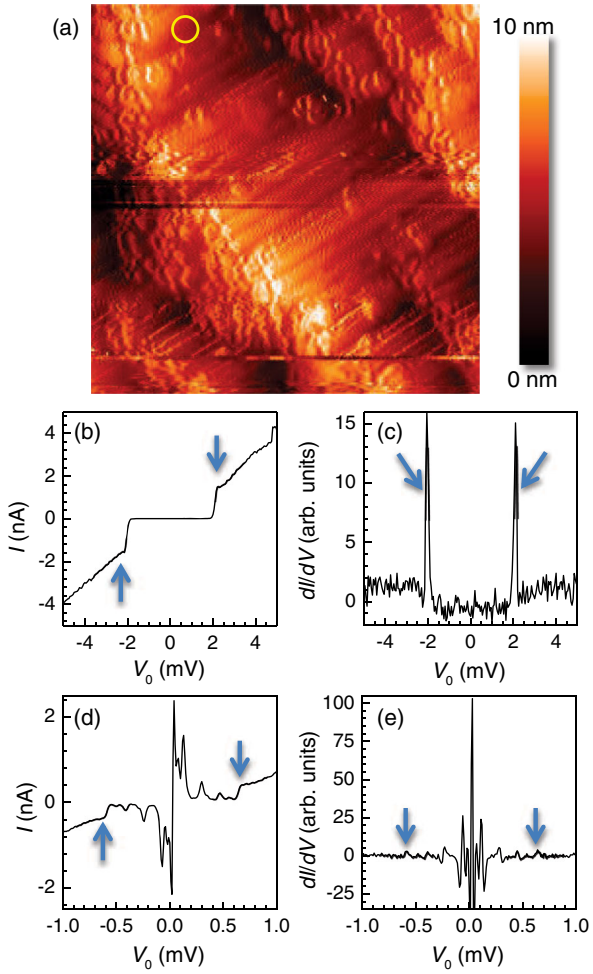

FIG. 3. (a) Typical topography of the Nb(100) surface using a Nb tip at 30 mK. The image size is 25×25 nm^2 with a corrugation of 6 nm and a rms roughness of 0.98 nm. (b) $I(V)$ and (c) dI/dV data, respectively, showing the full *S-I-S* gap (arrows, $\Delta_{S\text{-}I\text{-}S} = 2.08$ meV) at a junction resistance of $R_J = 16.7$ MΩ. Curves (d) and (e) show $I(V)$ and dI/dV data, respectively, of the fine subgap structure. Here the arrows mark the position of the smaller of the two gaps, most likely the tip gap, of $\Delta_{tip} = 0.61$ meV at $R_J = 10.0$ MΩ implying $\Delta_{sample} = 1.47$ meV. The yellow circle in (a) marks the region where the spectroscopic data are acquired.

IV. MEASUREMENT AND DISCUSSION

Figure 4 shows a series of conductance $G(V_0)$ curves taken with the inner STM tip at the position marked in Fig. 3(a) with applied microwaves of frequency $\omega/2\pi = f = 5.6$ GHz. Starting with zero microwave power, each successive curve is measured at a fixed microwave source amplitude (V_{ac}) that is increased in steps of 25 mV from 0 to 3 V. The bottom curve ($V_{ac} = 0$ V) shows a distinct conduction peak at zero bias, as expected, due to phase diffusion [23]. The weaker side structures are due to coupling to microwave modes in the environment and can, in principle, be described by $P(E)$

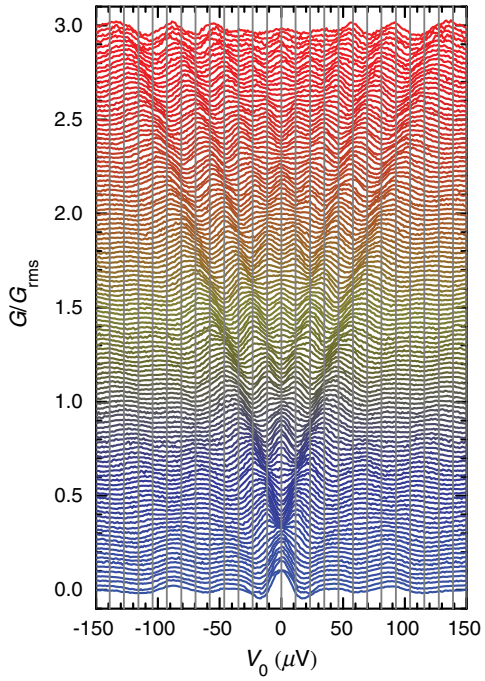

FIG. 4. Normalized measured conductance $G/G_{\rm rms}$ versus dc bias voltage V_0 taken at 30 mK with the inner Nb-Nb STM junction under irradiation by 5.6-GHz microwaves. The amplitude of the applied voltage $V_{\rm ac}$ varies from 0 V (blue) to 3.0 V (red) in steps of 25 mV. Successive curves are offset by 0.025 on the y axis. Vertical gray lines are spaced $\hbar\omega/2e = 11.6$ μV apart and coincide with emerging peaks in conductance, indicating that the charge of the carriers is $2e$. $G_{\rm rms}$ is the rms deviation of G of each trace.

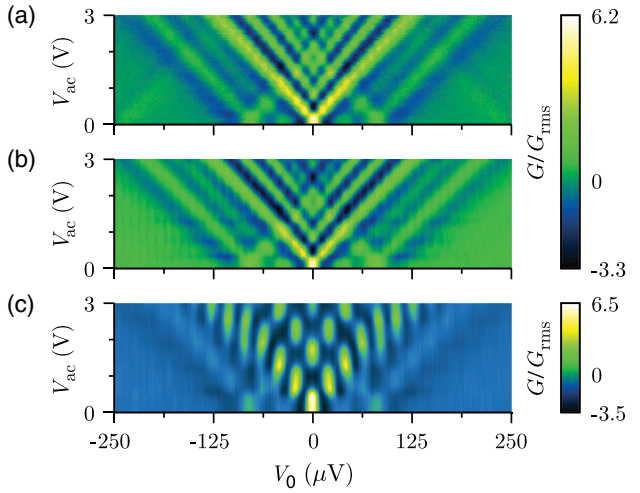

FIG. 5. (a) False color plot of data in Fig. 4 showing measured conductance $G/G_{\rm rms}$ versus dc bias voltage V_0 and applied microwave amplitude $V_{\rm ac}$ at a frequency of $f = 5.6$ GHz. (b) Simulated false color plot assuming charge carriers are Cooper pairs. The measured conductance curve in the absence of microwaves and Eq. (4a) are used to generate each successive curve, with $A_\mu = V_\mu/V_{\rm ac} \approx 6.5 \times 10^{-5}$. (c) Simulated false color plot assuming the charge carriers are quasiparticles with charge e. The measured conductance curve in the absence of microwaves and the equivalent of Eq. (1) are used to generate each successive curve with $A_\mu = 6.5 \times 10^{-5}$.

theory [26]. As the microwave amplitude increases, additional peaks appear in the conductance curve. The positions of the peaks coincide with the vertical gray lines spaced $\hbar\omega/2e = 11.6$ μeV apart (see Fig. 4). For each conductance curve of N points, we normalize by the standard deviation $G_{\rm rms} = \sqrt{1/(N-1)\sum_{n=1}^{N}(G_n - \bar{G})^2}$ of that curve to compensate for variations between curves due to the systematic decline in feature size for higher microwave amplitudes.

Figure 5(a) shows a false color plot of the data displayed in Fig. 4, while Fig. 5(b) shows for comparison the expected response for phase-incoherent pair tunneling based on Eq. (4a). To generate Fig. 5(b), we use the first line of conductance data measured in the absence of microwaves and generate each successive line of nonzero microwave amplitude by applying Eq. (4a). Each simulated curve is divided by its standard deviation $G_{\rm rms}$ to allow direct comparison with the data in Fig. 5(a). We note that the only fitting parameter is an overall scale factor $A_\mu \equiv V_\mu/V_{\rm ac}$: the ratio of the amplitude of the applied voltage across the junction V_μ to the amplitude $V_{\rm ac}$ at the source. For Fig. 5(b), we set $A_\mu = 6.5 \times 10^{-5}$.

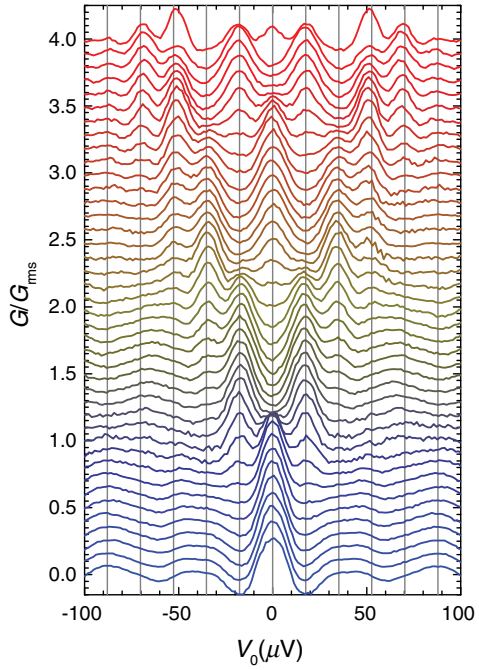

FIG. 6. Measured conductance $G/G_{\rm rms}$ versus dc bias voltage V_0 taken at 30 mK with the inner tip Nb-Nb STM junction under irradiation of $f = 8.5$ GHz microwaves. The amplitude of the applied microwaves $V_{\rm ac}$ is varied from 0 V (blue) to 4.0 V (red) in steps of 0.1 V. Successive curves are offset by 0.1 on the y axis. Vertical gray lines are spaced $\hbar\omega/2e = 17$ μeV apart. They coincide with high peaks in conductance, indicating that the charge of the carriers is $2e$.

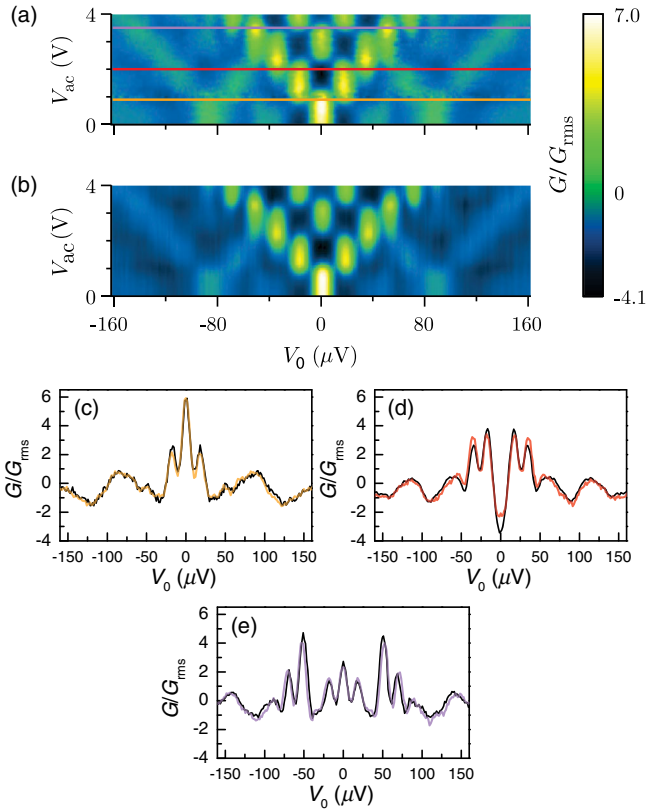

FIG. 7. (a) False color plot of Fig. 6 showing measured conductance $G/G_{\rm rms}$ versus dc bias voltage V_0 and applied microwave amplitude $V_{\rm ac}$ for a microwave frequency of $f = 8.5$ GHz. (b) Simulated false color plot for phase-incoherent pair tunneling generated using the measured conductance curve in the absence of microwaves and Eq. (4a) to generate each successive curve with $A_\mu = V_\mu/V_{\rm ac} \approx 3.5 \times 10^{-5}$. (c) Orange curve shows $G/G_{\rm rms}$ at $V_{\rm ac} = 0.9$ V, and black shows corresponding simulated curve from (b). (d) Red curve shows data at $V_{\rm ac} = 2.0$ V; black shows corresponding simulated curve from (b). (e) Purple curve shows data at $V_{\rm ac} = 3.5$ V, and black curve is the corresponding simulated curve from (b).

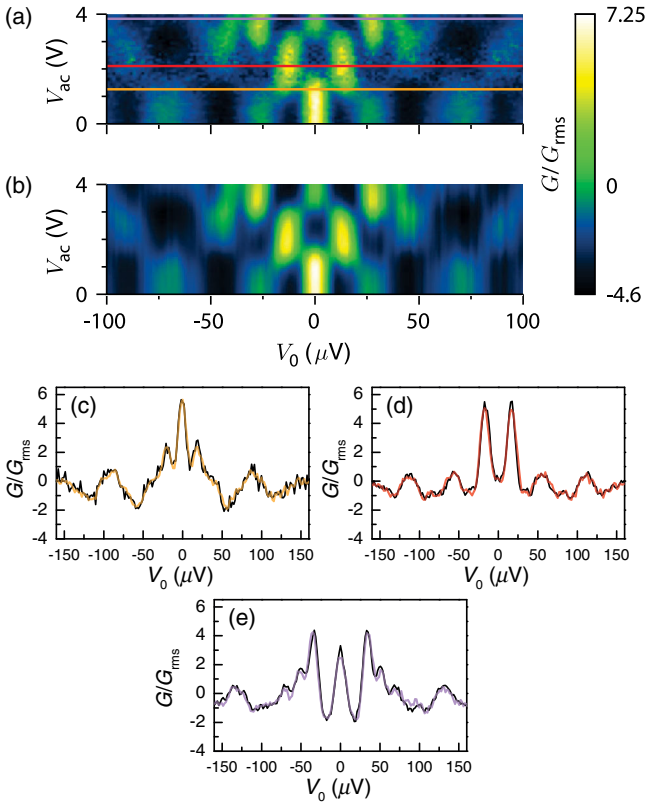

FIG. 8. (a) False color plot of measured conductance $G/G_{\rm rms}$ versus dc bias voltage V_0 and applied microwave amplitude $V_{\rm ac}$. Data are taken at 30 mK with outer STM tip. The microwave frequency is $f = 8.5$ GHz. Each horizontal line corresponds to a conductance curve with yellow representing the positive peaks and dark blue representing the negative dips. (b) Simulation of false color plot for phase-incoherent pair tunneling generated using the measured conductance curve in the absence of microwaves and Eq. (4a) to generate each successive curve with $A_\mu = V_\mu/V_{\rm ac} \approx 2.9 \times 10^{-5}$. (c)–(e) Line cuts similar to Fig. 7 showing data (color) and simulation (black) at $V_{\rm ac} = 1.3$, 2.1, and 3.9 V, respectively.

We see excellent agreement between Figs. 5(b) and 5(a), indicating that the current is due to phase-incoherent tunneling of pairs. In particular, the charge carriers are Cooper pairs because the voltage spacing between the split conductance peaks is $\hbar\omega/2e$. The $P(E)$ structures at $V_0 \approx \pm 30$ μV and $V_0 \approx \pm 80$ μV split in similar fashion and are, thus, also due to Cooper pairs. In contrast, Fig. 5(c) shows the corresponding simulation assuming the charge carriers are quasiparticles with charge e. The voltage spacing in Fig. 5(c) is twice that for Cooper pairs and disagrees strongly with the data.

We also measure the inner STM junction's response to $f = 8.5$ GHz microwaves at a different location on the sample ($\Delta_{\rm tip} = 0.625$ meV, $\Delta_{\rm sample} = 1.51$ meV). Since the spacing between the peaks should scale with frequency, they should be easier to resolve provided sufficient power reaches the junction. Figure 6 shows a series of normalized conductance curves measured as the applied microwave amplitude is increased from 0 to 4.0 V. The gray lines spaced by $\hbar\omega/2e = 17$ μeV once again coincide with the measured peaks. The corresponding false color map is shown in Fig. 7(a), and the simulated false color map based on the curve measured at zero microwave power and Eq. (4a) for pair tunneling is shown in Fig. 7(b). Figures 7(c)–7(e) show line sections through the data marked by the orange, red, and purple lines in Fig. 7(a) and the corresponding simulated curves from Fig. 7(b). The quantitative agreement is very good, consistent with the peaks being due to phase-incoherent tunneling of pairs and inconsistent with quasiparticles or Shapiro steps that will arise from phase-coherent tunneling of pairs.

To rule out the possibility that the observed effect of microwaves is a junction-specific phenomenon, the outer Nb tip in our dual-tip STM is used to confirm the results.

Here, the tip and sample gap are $\Delta_{tip} = 1.35$ meV and $\Delta_{sample} = 1.37$ meV, respectively. Figure 8(a) shows conductance measurements with the outer STM tip with $f = 8.5$ GHz microwave radiation. Close comparison of Figs. 7(a) (inner tip) and 8(a) (outer tip) reveal small differences. Since each tip of our STM has its own set of current and piezo leads, the resonant microwave frequencies associated with each circuit are different, leading to small differences in the $V_{ac} = 0$ V conductance curve. Nevertheless, we again find very good agreement between the data and Eq. (4a) [see Figs. 8(a)–(e)].

V. CONCLUSION

Subgap conductance features occur in voltage-biased SC STM junctions due to resonances in the junctions' electromagnetic environment. When microwave radiation is applied, the features evolve as the microwave voltage is increased. In our ultralow-temperature system, these features are due to *phase-incoherent* tunneling of Cooper pairs; phase-coherent tunneling of Cooper pairs is not consistent with the data. Theoretical fits to the highly resolved tunneling spectra allow us to exclude quasiparticle contributions to the tunneling current. In principle, a quasiparticle fraction of 2% or larger can be detected.

Photon-assisted tunneling with a JSTM allows the atomic-scale [28,31] identification of the charge of carriers that produce any sharp voltage-dependent features in conductance data. This technique can be implemented in other millikelvin STM systems with the "simple" addition of a microwave drive and the use of superconducting tips. While traditional STMs that rely on quasiparticle tunneling provide excellent spatial maps of various materials, they are insensitive to the origin of gap states. Our Josephson STM provides similar spatial maps of materials but additionally discerns the superconducting from quasiparticle currents.

There are several potential applications of a Josephson STM in a microwave field. It can aid in the discovery of new superconductors, as well as improve understanding of the behavior of superconductors near atomic-scale perturbations. Vortex cores, small normal regions, or the effects of single magnetic spins can be probed by mapping out the quasiparticle and Cooper-pair contributions to the current at the boundary of normal and SC regions of the samples. In addition, pseudogap states or other competing orders can be distinguished from superconductivity in spatially inhomogeneous highly correlated electron systems. Furthermore, this technique can be used to discern whether the zero-bias conductance peak in a topological superconductor arises from superconductivity or something more exotic such as the Majorana fermion [32]. Finally, the measurement technique may also provide a way to attain position-dependent measurements of local resonant absorption peaks, of interest when studying the effects of adsorbed molecules or resonant two-level systems [33–35] in quantum computing applications.

ACKNOWLEDGMENTS

The authors acknowledge many useful conversations with P. Barbara, B. Palmer, and B. Suri. Portions of this work are funded by the National Science Foundation under Grant No. DMR-0605763 and the Laboratory for Physical Sciences.

[1] J. G. Rodrigo, H. Suderow, and S. Vieira, On the use of STM superconducting tips at very low temperatures, Eur. Phys. J. B **40**, 483 (2004).

[2] I. Guillamon, H. Suderow, S. Vieira, and P. Rodiere, Scanning tunneling spectroscopy with superconducting tips of Al, Physica (Amsterdam) **468C**, 537 (2008).

[3] Y. Noat, T. Cren, V. Dubost, S. Lange, F. Debontridder, P. Toulemonde, J. Marcus, A. Sulpice, W. Sacks, and D. Roditchev, Disorder effects in pnictides: A tunneling spectroscopy study, J. Phys. Condens. Matter **22**, 465701 (2010).

[4] J. Rodrigo, V. Crespo, and S. Vieira, Josephson current at atomic scale: Tunneling and nanocontacts using a STM, Physica (Amsterdam) **437C–438C**, 270 (2006).

[5] A. Kohen, Y. Noat, T. Proslier, E. Lacaze, M. Aprili, W. Sacks, and D. Roditchev, Fabrication and characterization of scanning tunneling microscopy superconducting Nb tips having highly enhanced critical fields, Physica (Amsterdam) **419C**, 18 (2005).

[6] N. Bergeal, Y. Noat, T. Cren, T. Proslier, V. Dubost, F. Debontridder, A. Zimmers, D. Roditchev, W. Sacks, and J. Marcus, Mapping the superconducting condensate surrounding a vortex in superconducting V_3Si using a superconducting MgB_2 tip in a scanning tunneling microscope, Phys. Rev. B **78**, 140507 (2008).

[7] B. Jäck, M. Eltschka, M. Assig, A. Hardock, M. Etzkorn, C. R. Ast, and K. Kern, A nanoscale gigahertz source realized with Josephson scanning tunneling microscopy, Appl. Phys. Lett. **106**, 013109 (2015).

[8] O. Naaman, W. Teizer, and R. C. Dynes, The fabrication of reproducible superconducting scanning tunneling microscope tips, Rev. Sci. Instrum. **72**, 1688 (2001).

[9] B. D. Josephson, Possible new effects in superconductive tunnelling, Phys. Lett. **1**, 251 (1962).

[10] Y. M. I. Anchenko and L. A. Zil'berman, The Josephson effect in small tunnel contacts, Sov. Phys. JETP **6**, 1272 (1969).

[11] H. Kimura, R. P. Barber, S. Ono, Y. Ando, and R. C. Dynes, Scanning Josephson Tunneling Microscopy of Single-Crystal $Bi_2Sr_2CaCu_2O_{8+\delta}$ with a Conventional Superconducting Tip, Phys. Rev. Lett. **101**, 037002 (2008).

[12] E. L. Wolf, A. Chang, Z. Y. Rong, Y. M. Ivanchenko, and F. Lu, Direct STM mapping of the superconducting energy gap in single crystal $Bi_2Sr_2CaCu_2O_{8+x}$, J. Supercond. **7**, 355 (1994).

[13] C. Howald, P. Fournier, and A. Kapitulnik, Inherent inhomogeneities in tunneling spectra of $Bi_2Sr_2CaCu_2O_{8-x}$ crystals in the superconducting state, Phys. Rev. B **64**, 100504 (2001).

[14] O. Fischer, M. Kugler, C. Berthod, and C. Renner, Scanning tunneling spectroscopy of high-temperature superconductors, Rev. Mod. Phys. **79**, 353 (2007).
[15] P. K. Tien and J. P. Gordon, Multiphoton Process observed in the interaction of microwave fields with the tunneling between superconductor films, Phys. Rev. **129**, 647 (1963).
[16] J. N. Sweet and G. I. Rochlin, Microwave-photon-assisted tunneling in Sn-I-Sn superconducting tunnel junctions, Phys. Rev. B **2**, 656 (1970).
[17] L. P. Kouwenhoven, S. Jauhar, K. McCormick, D. Dixon, P. L. McEuen, Y. V. Nazarov, N. C. van der Vaart, and C. T. Foxon, Photon-assisted tunneling through a quantum dot, Phys. Rev. B **50**, 2019 (1994).
[18] J. M. Hergenrother, M. T. Tuominen, J. G. Lu, D. C. Ralph, and M. Tinkham, Charge transport and photon-assisted tunneling in the NSN single-electron transistor, Physica (Amsterdam) **203B**, 327 (1994).
[19] Y. Nakamura, C. D. Chen, and J. S. Tsai, Observation of photon-assisted Josephson-quasiparticle current, Czech. J. Phys. **46**, 2301 (1996).
[20] R. J. Fitzgerald, J. M. Hergenrother, S. L. Pohlen, and M. Tinkham, Crossover from photon-assisted tunneling to classical behavior in single-electron transistors, Phys. Rev. B **57**, 9893 (1998).
[21] S. E. de Graaf, J. Leppäkangas, A. Adamyan, A. V. Danilov, T. Lindström, M. Fogelström, T. Bauch, G. Johansson, and S. E. Kubatkin, Charge Qubit Coupled to an Intense Microwave Electromagnetic Field in a Superconducting Nb Device: Evidence for Photon-Assisted Quasiparticle Tunneling, Phys. Rev. Lett. **111**, 137002 (2013).
[22] G. Falci, V. Bubanja, and G. Schön, Quasiparticle and Cooper pair tunneling in small capacitance Josephson junctions, Z. Phys. B **85**, 451 (1991).
[23] M. Tinkham, *Introduction to Superconductivity* (McGraw-Hill, Inc., New York, 1996).
[24] S. Shapiro, Josephson Currents in Superconducting Tunneling: The Effect of Microwaves and Other Observations, Phys. Rev. Lett. **11**, 80 (1963).
[25] D. V. Averin and K. K. Likharev, Coulomb blockade of single-electron tunneling, and coherent oscillations in small tunnel junctions, J. Low Temp. Phys. **62**, 345 (1986).
[26] G.-L. Ingold, H. Grabert, and U. Eberhardt, Cooper-pair current through ultrasmall Josephson junctions, Phys. Rev. B **50**, 395 (1994).
[27] A. Roychowdhury, M. A. Gubrud, R. Dana, J. R. Anderson, C. J. Lobb, F. C. Wellstood, and M. Dreyer, A 30 mK, 13.5 T scanning tunneling microscope with two independent tips, Rev. Sci. Instrum. **85**, 043706 (2014).
[28] A. Roychowdhury, Ph.D. thesis, University of Maryland, 2014.
[29] Agilent N5183A microwave analog signal generator.
[30] Stanford Research Systems SR830 lock-in amplifier.
[31] A. Roychowdhury, R. Dana, M. Dreyer, J. R. Anderson, C. J. Lobb, and F. C. Wellstood, Plasma etching of superconducting niobium tips for scanning tunneling microscopy, J. Appl. Phys. **116**, 014308 (2014).
[32] S. R. Elliott and M. Franz, Colloquium: Majorana fermions in nuclear, particle, and solid-state physics, Rev. Mod. Phys. **87**, 137 (2015).
[33] M. S. Khalil, F. C. Wellstood, and K. D. Osborn, Loss dependence on geometry and applied power in superconducting coplanar resonators, IEEE Trans. Appl. Supercond. **21**, 879 (2011).
[34] A. M. Holder, K. D. Osborn, C. J. Lobb, and C. B. Musgrave, Bulk and Surface Tunneling Hydrogen Defects in Alumina, Phys. Rev. Lett. **111**, 065901 (2013).
[35] A. L. Burin, A. O. Maksymov, and K. D. Osborn, Quantum coherent manipulation of two-level systems in superconducting circuits, Supercond. Sci. Technol. **27**, 084001 (2014).